Dalton Transactions

ROYAL SOCIETY OF CHEMISTRY

PAPER

View Article Online
View Journal | View Issue

Cite this: *Dalton Trans.*, 2023, **52**, 8956

A bis-calix[4]arene-supported $[Cu^{II}_{16}]$ cage†

Lucinda R. B. Wilson, [a] Marco Coletta, [a] Mukesh K. Singh, [a] Simon J. Teat, [b] Adam Brookfield,[c] Muralidharan Shanmugam,[c] Eric J. L. McInnes, [c] Stergios Piligkos, *[d] Scott J. Dalgarno *[e] and Euan K. Brechin *[a]

Received 15th May 2023,
Accepted 8th June 2023

DOI: 10.1039/d3dt01448g

rsc.li/dalton

Reaction of 2,2′-bis-*p*-^{t}Bu-calix[4]arene (H_8L) with $Cu(NO_3)_2{\cdot}3H_2O$ and *N*-methyldiethanolamine (Me-deaH$_2$) in a basic dmf/MeOH mixture affords $[Cu^{II}_{16}(L)_2(Me\text{-}dea)_4(\mu_4\text{-}NO_3)_2(\mu\text{-}OH)_4(dmf)_{3.5}(MeOH)_{0.5}(H_2O)_2](H_6L){\cdot}16dmf{\cdot}4H_2O$ (**4**), following slow evaporation of the mother liquor. The central core of the metallic skeleton describes a tetracapped square prism, $[Cu_{12}]$, in which the four capping metal ions are the Cu^{II} ions housed in the calix[4]arene polyphenolic pockets. The $[Cu^{II}_8]$ square prism is held together "internally" by a combination of hydroxide and nitrate anions, with the *N*-methyldiethanolamine co-ligands forming dimeric $[Cu^{II}_2]$ units which edge-cap above and below the upper and lower square faces of the prism. Charge balance is maintained through the presence of one doubly deprotonated H_6L^{2-} ligand per $[Cu_{16}]$ cluster. Magnetic susceptibility measurements reveal the predominance of strong antiferromagnetic exchange interactions and an $S = 1$ ground state, while EPR is consistent with a large zero-field splitting.

Introduction

Interest in the magnetic behaviour of polymetallic complexes of Cu^{II} can be traced back to studies of copper acetate[1] in the 1950s and the subsequent magneto-structural correlations developed for $[Cu_2]$ dimers bridged by hydroxides, halides and azides.[2–6] Later studies examined larger, more complex structure types such as $[Cu_3]$ triangles,[7] $[Cu_4]$ cubes,[8] $[Cu]_n$ chains[9] and heterometallic species containing transition metal[10] or lanthanide metal centres.[11] Many of these studies revealed fascinating magnetic behaviours, such as the spin frustration prevalent in equilateral triangles[12] which represent the simplest molecular analogues of the kagome lattice,[13] a topology also of relevance in multicopper oxidases.[14]

A search of the Cambridge Structural Database (CSD) reveals there are several hundred homometallic O/N-bridged Cu^{II} clusters deposited that possess a nuclearity of two or more, with the largest being $[Cu_{44}]$, reported in 2004.[15] However, as nuclearity increases this number decreases significantly – for example there are less than twenty with a nuclearity of twenty or more. A seemingly ideal ligand framework for housing the Jahn–Teller (JT) distorted octahedral Cu^{II} ion is *p*-^{t}Bu-calix[4]arene ($H_4TBC[4]$; Fig. 1A), its tetraphenolic pocket being perfectly suited to accommodating four short equatorial bonds. Despite this, and the success of $H_4TBC[4]$ in the coordination chemistry of the JT distorted octahedral Mn^{III} ion,[16] there are just three homometallic Cu^{II} compounds known. The first two, $[Cu^{II}_9(OH)_3(TBC[4])_3Cl_2(dmso)_{5.5}(EtOH)_{0.5}][Cu^{I}Cl_2]$ (**1**)

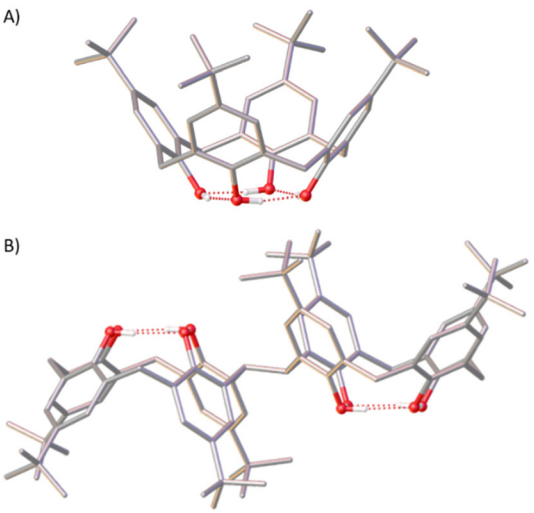

Fig. 1 Single crystal X-ray structures of $H_4TBC[4]$ (A) and H_8L (B). Colour code C = grey, O = red, H = white.

[a]*EastCHEM School of Chemistry, The University of Edinburgh, David Brewster Road, Edinburgh, Scotland, EH9 3FJ, UK. E-mail: ebrechin@ed.ac.uk*
[b]*Station 11.3.1, Advanced Light Source, Lawrence Berkeley National Laboratory, 1 Cyclotron Road, Berkeley, CA 94720, USA*
[c]*School of Chemistry, The University of Manchester, Oxford Road, Manchester, England, M13 9PL, UK. E-mail: eric.mcinnes@manchester.ac.uk*
[d]*Department of Chemistry, University of Copenhagen, Universitetsparken 5, DK-2100 Copenhagen, Denmark. E-mail: piligkos@chem.ku.dk*
[e]*Institute of Chemical Sciences, Heriot-Watt University, Riccarton, Edinburgh, Scotland, EH14 4AS, UK. E-mail: S.J.Dalgarno@hw.ac.uk*

†Electronic supplementary information (ESI) available: Additional figures and further computational details. CCDC 2101166. For ESI and crystallographic data in CIF or other electronic format see DOI: https://doi.org/10.1039/d3dt01448g

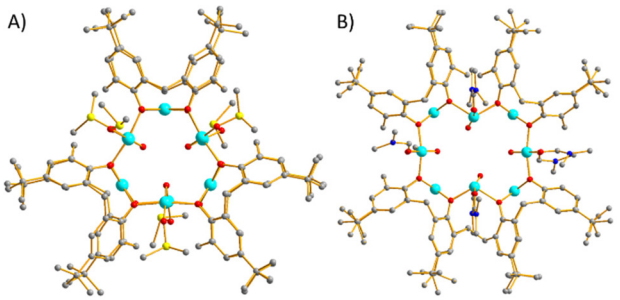

Fig. 2 Partial single crystal X-ray structures of **1** (A) and **3** (B). The disordered central Cu ion in **3** has been omitted. Colour code: C = grey, O = red, N = dark blue, S = yellow, Cu^{II} = light blue. H atoms and co-crystallised solvent/anions omitted for clarity.

and $[Cu^{II}_9(OH)_3(TBC[4])_3(NO_3)_2(dmso)_6](NO_3)$ (**2**) (Fig. 2A), are isostructural and were both reported in the same paper.[17] Their metallic skeletons describe tricapped trigonal prisms in which $[Cu\text{-}TBC[4]]^{2-}$ moieties act as metalloligands that encapsulate an hydroxide-bridged $[Cu_6]$ trigonal prism.

Extension of this chemistry to examine the coordination behaviour of the related ligand 2,2′-bis-*p*-^{t}Bu-calix[4]arene (H_8L),[18] in which two $H_4TBC[4]$s are linked *via* a methylene bridge (Fig. 1B), affords the larger, but related $[Cu^{II}_{13}(L)_2(NO_3)(\mu\text{-}OH)_8(dmf)_7](OH)$ (**3**) whose metallic skeleton describes a centred, tetracapped square prism (Fig. 2B).[19] The expansion from $[Cu_9]$ to $[Cu_{13}]$ is a result of the conformational flexibility (ring inversion) of H_8L which, upon metal coordination, provides an organic skeleton with eight proximal phenolic O-atoms. In order to explore this reaction space further we have adapted the synthesis of complex **3** to include a flexible bridging co-ligand, *N*-methyldiethanolamine (Me-deaH$_2$), which enables the formation of the larger complex $[Cu^{II}_{16}(L)_2(Me\text{-}dea)_4(\mu_4\text{-}NO_3)_2(\mu\text{-}OH)_4(dmf)_{3.5}(MeOH)_{0.5}(H_2O)_2](H_6L)\cdot16dmf\cdot4H_2O$ (**4**) whose metallic skeleton is also based on a multiply-capped square prism.

Experimental

Synthesis

$Cu(NO_3)_2\cdot3H_2O$ was purchased from commercial suppliers and used without further purification. 2,2′-Bis-*p*-^{t}Bu-calix[4]arene (H_8L) was prepared as previously described.[18]

$[Cu^{II}_{16}(L)_2(Me\text{-}dea)_4(\mu_4\text{-}NO_3)_2(\mu\text{-}OH)_4(dmf)_{3.5}(MeOH)_{0.5}(H_2O)_2](H_6L)\cdot16dmf\cdot4H_2O$ (4). $Cu(NO_3)_2\cdot3H_2O$ (1 mmol, 250 mg), H_8L (0.154 mmol, 200 mg) and Me-deaH$_2$ (0.174 mmol, 20 μL) were dissolved in a 1 : 1 dmf/MeOH mixture (24 mL) and stirred for 10 minutes. An excess of NEt_3 (2.87 mmol, 400 μL) was added and the resulting brown solution was stirred for 2 hours and then filtered. Slow evaporation of the mother liquor afforded dark brown crystals suitable for X-ray diffraction. Elemental analysis calculated for (**4**), $C_{343}H_{510.5}Cu_{16}N_{25.5}O_{68}$: C, 58.06%; H, 7.25%: N, 5.03%. Found C, 57.82%; H, 6.93; N, 4.69%.

X-ray crystallography

Diffraction data for **4** were collected on a Bruker D8 diffractometer equipped with a PHOTON 100 detector and operating with synchrotron radiation (0.7749 Å). Crystal data for **4** (CCDC 2101166†): $C_{343}H_{510.5}Cu_{16}N_{25.5}O_{68}$, M = 7095.88 g mol^{-1}, triclinic, space group $P\bar{1}$ (no. 2), a = 21.4369(9) Å, b = 21.9078(9) Å, c = 22.0660(9) Å, α = 105.596(3)°, β = 111.468(2)°, γ = 95.527(3)°, V = 9067.1(7) Å^3, Z = 1, T = 100(2) K, μ(synchrotron) = 1.251 mm^{-1}, $D_{calc.}$ = 1.300 g cm^{-3}, 56 519 reflections measured ($4.312° \leq 2\Theta \leq 47.784°$), 21 580 unique ($R_{int}$ = 0.0705, R_{sigma} = 0.0826) which were used in all calculations. The final R_1 was 0.0566 ($I > 2\sigma(I)$) and wR_2 was 0.1551 (all data).

Magnetic data

Magnetic susceptibility and magnetisation data were collected on a powdered microcrystalline sample of **4** using a Quantum Design PPMS Dynacool. Susceptibility data were collected in the T = 2–300 K range under and applied magnetic field, B = 0.1 T. Magnetisation data were collected in the T = 2–10 K and B = 0.5–9.0 T ranges. A unit cell check was performed prior to measurement.

EPR spectroscopy

EPR spectra were measured on powder and solution (CH_2Cl_2/toluene) samples of **4**, at 10 and 20 K and over the 0–1.8 T field range, on a Bruker EMXPlus spectrometer.

Computational details

Density functional theory in conjunction with the broken symmetry approach[20] has been used to estimate the magnetic exchange interactions in complex **4** employing Gaussian 09.[21] The hybrid B3LYP functional[22] together with Ahlrichs TZV basis set for was used for the Cu atoms, the SVP basis set for O and N atoms, and the SV basis set for C and H atoms.[23] This methodology has been shown to reproduce experimental magnetic exchange interactions accurately.[24]

Results and discussion

Reaction of H_8L with $Cu(NO_3)_2\cdot3H_2O$ and Me-deaH$_2$ in a basic dmf/MeOH mixture affords single crystals of formula $[Cu^{II}_{16}(L)_2(Me\text{-}dea)_4(\mu_4\text{-}NO_3)_2(\mu\text{-}OH)_4(dmf)_{3.5}(MeOH)_{0.5}(H_2O)_2](H_6L)\cdot16dmf\cdot4H_2O$ (**4**, Fig. 3 and 4), following slow evaporation of the mother liquor. The crystals were found to be in a triclinic cell and structure solution was carried out in the space group $P\bar{1}$. The asymmetric unit (ASU) comprises half of the formula.

The metallic skeleton describes a tetracapped (Cu1–2 and symmetry equivalent) square prism (Cu3–6) in which the 'upper' and 'lower' square faces (as drawn in Fig. 4B) are edge-capped by a $\{Cu_2\}$ (Cu7–8) moiety. The Cu ions in the upper and lower faces of the square prism are connected to each other by four μ-OH ions to form a $[Cu_8(OH)_4]^{12+}$ central unit (Fig. S1†). The four face-capping Cu ions are housed in the polyphenolic pockets of the two fully deprotonated bis-calixar-

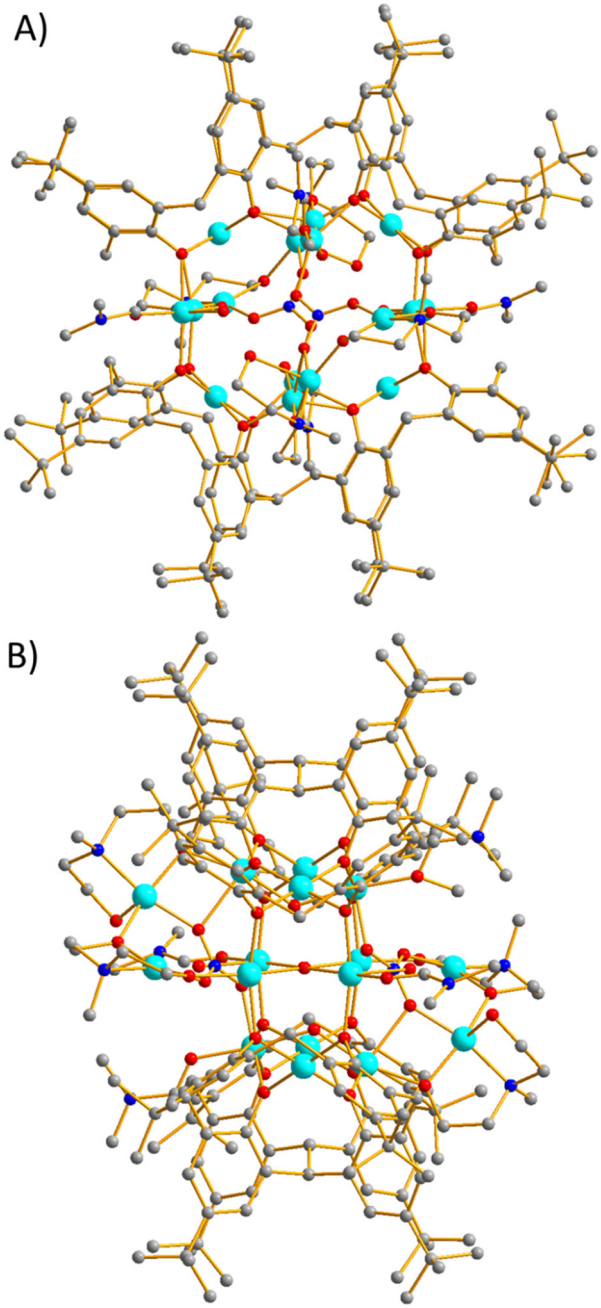

Fig. 3 Orthogonal views of the molecular structure of the cation of **4** shown 'face-on' (A) and 'side-on' (B). Colour code: C = grey, O = red, N = dark blue, Cu^{II} = light blue. H atoms and co-crystallised solvent/anions omitted for clarity.

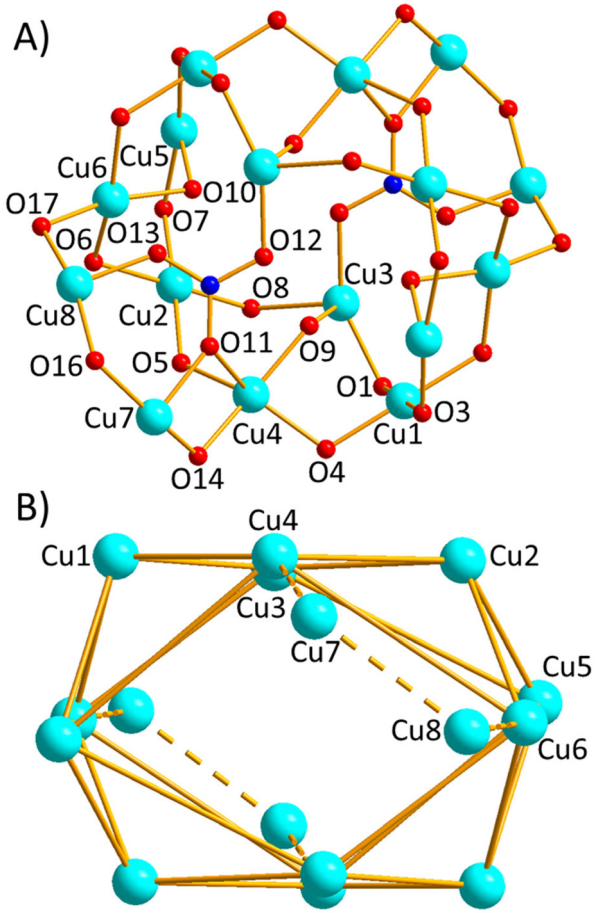

Fig. 4 Cluster core (A) and metallic skeleton (B) of **4**. Colour code: O = red, N = dark blue, Cu^{II} = light blue. The eight Cu ions in the square prism are Cu3–6 and symmetry equivalents. The four face-capping Cu ions are Cu1–2. The four edge-capping Cu ions are Cu7–8.

ene ligands whose O-atoms further bridge to the Cu ions in the square prism (Cu3–Cu6; Fig. S1 and S2†). The L^{8-} ligands thus wrap around the four square faces of the prism in the 'equatorial' plane (as drawn in Fig. 1A), completely encapsulating the $[Cu_8(OH)_4]^{12+}$ central unit. The 'upper' and 'lower' faces of the prism are connected to the $\{Cu_2\}$ edge-cap by a μ_4-bridging NO_3^- ion which connects Cu3–4 to Cu7–8. The latter are further bridged to each other and the Cu ions on the vertices of the square prism by two Me-dea^{2-} ligands that bond in two different ways. The first μ_3-bridges, using one O-arm (O16) to link between Cu7–Cu8 and the other (O17) to link between Cu8 and Cu6 in the square prism. The second chelates to Cu7 with one O-arm terminally coordinated (O15) and one arm (O14) bridging to Cu4 in the square prism.

The Cu ions (Cu1–2) that sit in the tetraphenolic pocket of L^{8-} are square planar $\{CuO_4\}$ with a fifth, longer contact to a disordered molecule of dmf that fills the calixarene cavity. The Cu ions in the square prism (Cu3–6) are all five coordinate and in distorted square pyramidal geometry, the remaining sites on Cu3 and Cu5 being occupied by dmf/H_2O molecules. The Cu ions in the edge-capping $\{Cu_2\}$ moiety (Cu7, Cu8) bonded to the Me-dea^{2-} ligands are five-coordinate, square pyramidal $\{CuO_4N\}$, and four-coordinate, square planar $\{CuO_3N\}$, respectively.

The complex displays numerous intra- and inter-molecular H-bonding interactions (Fig. S3–S6†). The water molecule bonded to Cu5 is H-bonded to two O-atoms of the nitrate anion (O19···O12/O11, ~2.83–3.01 Å). O12 is also H-bonded to a μ-OH ion (O12···O9, ~2.95 Å), and the third O-atom in the nitrate anion (O13) is H-bonded to a dmf molecule bonded to

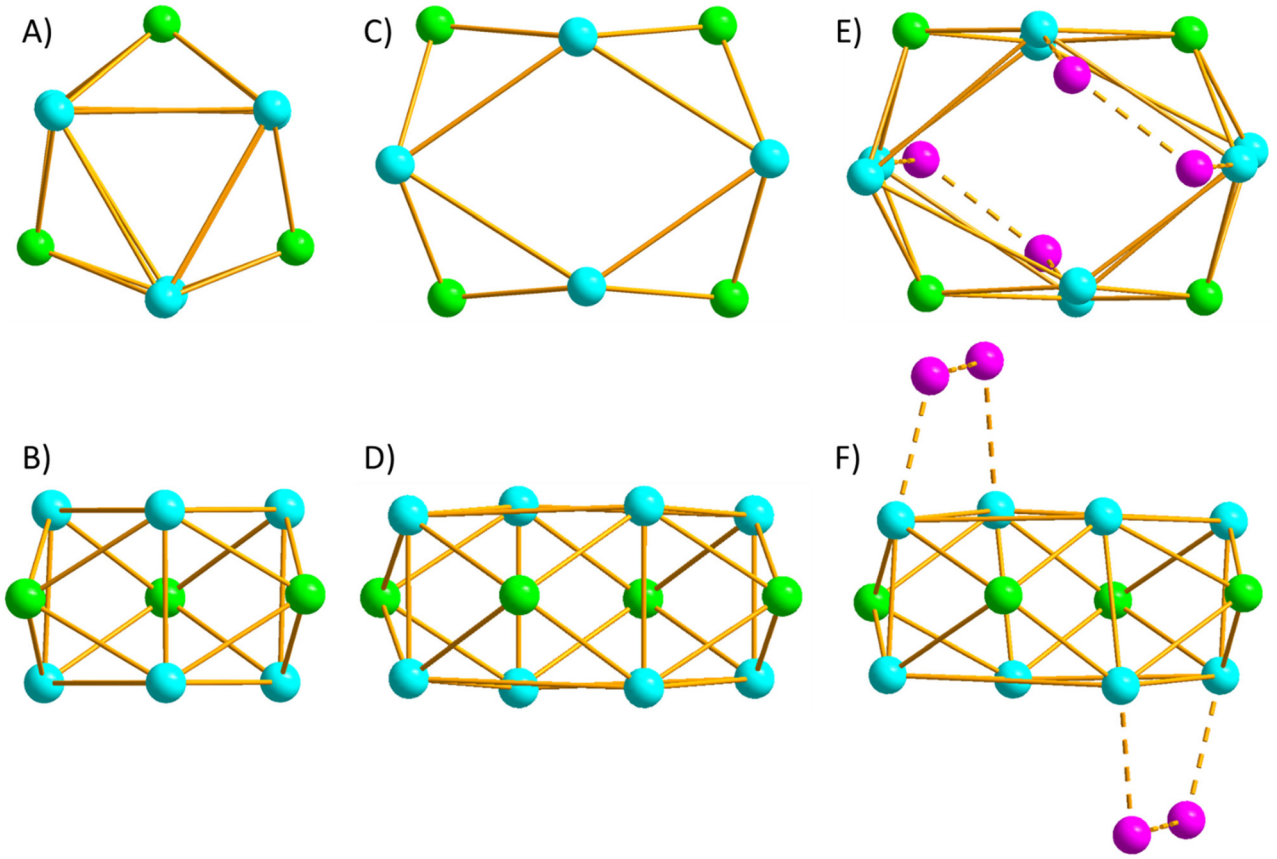

Fig. 5 A comparison of the metallic skeletons of [Cu_9] (**1–2**, A and B), [Cu_{13}] (**3**, C and D) and [Cu_{16}] (**4**, E and F). The central, distorted Cu ion in [Cu_{13}] has been removed to aid comparison. [Cu_9] describes a tricapped trigonal prism, [Cu_{13}] a (centred) tetracapped square prism, and [Cu_{16}] a tetracapped square prism containing two additional {Cu_2} edge-caps. The Cu ions in the prisms are in light blue, those housed in the tetraphenolic calixarene pocket in green and the edge-caps in pink.

Cu3 (O13···O18, ~3.00 Å). There is also a complex H-bonding network in the region of one of the two Me-dea^{2-} co-ligands. The O-atom (O15) belonging to the Me-dea^{2-} ligand supporting Cu7 is H-bonded to a H_2O molecule of crystallisation (O15···O21, ~2.62 Å). The latter is also interacting with the lower-rim oxygen atom of the co-crystallised H_6L^{2-} ligand (O21···O26, ~2.72 Å). Upon symmetry expansion, it is possible to appreciate the importance of this network of H-bonds as it dictates the way compound **4** and the co-crystallised molecules pack, through the formation of H-bonded chains (Fig. S3–S6†). The [Cu_{16}] cluster is surrounded at its four 'corners' by co-crystallised H_6L^{2-}. This doubly deprotonated molecule affords overall charge balance, and although there are waters of crystallisation present (and therefore potentially OH^- counter anions), we favour the presence of this dianion for two reasons. (1) The inter-molecular interactions discussed above; (2) refinement suggests each TBC[4] moiety in H_6L^{2-} is singly deprotonated, consistent with the highly acidic nature of H_4TBC[4] hydroxyl groups reported in literature.[25] The clusters are well isolated from each other, with the closest Cu···Cu distance being >12 Å between the Cu8 ions of distinct molecules. A search of the CSD shows that there are a total of thirteen [Cu^{II}_{16}] clusters known, none of which have a topology similar to **4**.[26]

A comparison of the metallic skeletons of [Cu_9], [Cu_{13}] and [Cu_{16}] (Fig. 5) shows some striking similarities. [Cu_9] is a tricapped trigonal prism in which the square faces are all capped by a Cu ion housed in the pocket of a TBC[4] moiety with halide/nitrate anions capping the upper/lower triangular faces. [Cu_{13}] is a centred, tetracapped square prism in which the 'equatorial' square faces are all capped by a Cu ion housed in the pocket of a TBC[4] moiety with nitrate anions capping the upper/lower triangular faces. [Cu_{16}] has a structure analogous to [Cu_{13}] but without the central Cu ion, and with two additional {Cu_2} edge-capping moieties introduced through the presence of a co-ligand. These structural similarities reflect the dominant, structure-directing influence of the calix[4]arene ligands.

Magnetic measurements

Direct current magnetic susceptibility (χ) studies were performed on a polycrystalline sample of **4** over the temperature range T = 2–300 K, in an applied magnetic field B = 0.1 T (Fig. 6), where $\chi = M/B$ and M is the magnetisation. At 300 K, the χT value of 5.9 cm^3 mol^{-1} K is below the expected value for

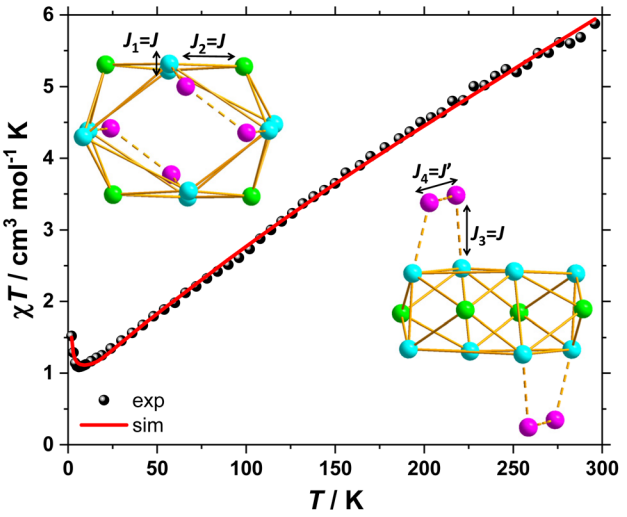

Fig. 6 Experimental χT *versus* T data for **4** measured in the T = 2–300 K temperature range in an applied field, B = 0.1 T.

spin-only contributions to the susceptibility for a $[Cu^{II}_{16}]$ unit (7.26 cm^3 mol^{-1} K, g = 2.2; 6.00 cm^3 mol^{-1} K, g = 2.0). Upon cooling, the χT product decreases rapidly until approximately T = 10 K where it reaches 1.1 cm^3 mol^{-1} K, wherefrom it increases upon further cooling reaching a value of 1.5 cm^3 mol^{-1} K at 2 K. The data are therefore suggestive of the presence of competing exchange interactions, in agreement with the range of Cu–O–Cu angles present, and previous magneto-structural correlations developed for smaller O-bridged Cu^{II} clusters.[1–6]

The quantitative interpretation of the temperature dependence of the χT product of **4** was performed by numerically fitting the experimental data to the full matrix representation of spin-Hamiltonian (1), of dimension 65 536 by 65 356, by use of the Levenberg–Marquardt algorithm.[27]

$$\hat{H} = \mu_B B \sum_i g_i \hat{S}_i - 2 \sum_{i,j>i} J_{ij} \hat{S}_i \cdot \hat{S}_j \qquad (1)$$

where the indices refer to the constituent Cu^{II} ions, μ_B is the Bohr magneton, g is the g-factor, $\hat{S}$ is a spin operator and J_{ij} is the bilinear pairwise isotropic exchange interaction parameter. Based on the structure of **4**, four different isotropic exchange parameters could be considered to fit the experimental temperature dependence of the χT product (Fig. 6, insets).

We employed irreducible tensor operator algebra to block-diagonalise the matrix representation of spin-Hamiltonian (1),[28] fixing the g factor for all Cu^{II} centres to g = 2, affording only the four different isotropic exchange parameters as free fit parameters. This resulted in very good agreement with the experimental data with the best-fit parameters J_1, J_2 and J_3 being strongly antiferromagnetic (AF), *ca.* −70 to −100 cm^{-1}, and J_4 being ferromagnetic (F), *ca.* +20 cm^{-1}. However, all these exchange parameters are strongly correlated, with only the correlation coefficients between J_4 and the others being less than 95%. Use of a single exchange parameter fails to satisfactorily reproduce the experimental data at all temperature regimes. Use of a model containing two different exchange parameters ($J_{1-3} = J, J_4 = J'$; Fig. 6, insets) results in a very good agreement with the experimental data (Fig. 6), with J = −122 ± 12 cm^{-1} and J' = 22 ± 8 cm^{-1}, with a correlation coefficient of 87%. With these best-fit parameters the ground spin-state of **4** is an S = 1 spin-state, with excited S = 0, 0 and 2 states lying 23, 35 and 46 cm^{-1} above the ground state, respectively, followed by a quasi-continuum of states (Fig. 7). We note that the exchange constant in the $[Cu_{12}]$ prism of **4** is similar to the values found in $[Cu_{13}]$ (**3**), which are all AF and in the range $-66 \leq J \leq -84$ cm^{-1}.[19] Employing the same isotropic model to fit the VTVB magnetisation data of **4** was not possible. This is because the VTVB magnetisation of **4** presents significant nesting (Fig. S7†) when plotted against B/T, which indicates anisotropy splittings of the same order of magnitude as the experimental conditions (T = 2 to 10 K and B = 1 to 9 T). Given that individual Cu^{II} centres are devoid of anisotropy (bar the g-factor), the observed anisotropy splittings can only originate (within the spin-Hamiltonian formalism) from magnetic exchange.[29] The experimental data do not allow for the determination of these exchange contributions to anisotropy.

Given the relatively well-isolated S = 1 ground state evidenced by the magnetic data and modelling, we attempted to probe this state by EPR spectroscopy at low temperatures. Spectra measured at 10 K and over the 0–1.8 T magnetic field range, at both X- and Q-band frequencies, only gave weak signals that could be attributed to small amounts of monomeric Cu^{II} species. This indicates that the zero-field splitting (ZFS) of the S = 1 state is significantly larger than the microwave frequencies applied. In order to estimate the ZFS, attempts were made to fit the VTVB magnetisation data to an isolated S = 1 model: while these fits were not entirely satisfactory (Fig. S7†) they indicate an axial ZFS parameters (D) of several cm^{-1}. This would be consistent with **4** being EPR silent

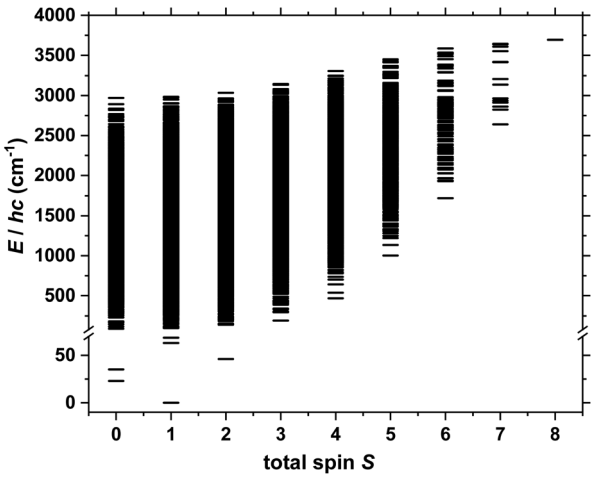

Fig. 7 Energy spectrum of **4** calculated from the fit of the susceptibility data, as described in the text. The ground spin-state of **4** is an S = 1 spin-state, with excited S = 0, 0 and 2 states lying 23, 35 and 46 cm^{-1} above the ground state.

under the measurement conditions. Given the lack of single-ion ZFS for Cu^{II}, the origin of such a ZFS must lie in anisotropic components of the exchange interaction.[29] Although a ZFS in the region of several cm^{-1} would be unusual for a Cu cluster, the project coefficients of anisotropic exchange are larger for lower total spins,[28] which may provide an explanation given that the ground state of **4** is the lowest possible total spin. It is more usual for Cu clusters to either give rise to a diamagnetic ground state or a high spin state, so there are few data to compare this against.

Theoretical studies

In order to analyse the sign and magnitude of the exchange interactions in more detail we have constructed three pentametallic models (**4A**, **4B**, **4C**) and one bimetallic model (**4D**) based on the X-ray structure of **4** to determine twelve exchange interactions (Fig. S8†). These are given in Table S2† and consist of ten antiferromagnetic interactions in the range $-3.9 < J < -55.7$ cm^{-1}, and two weakly ferromagnetic interactions in the range $+2.6 < J < +6.9$ cm^{-1}. The strongest antiferromagnetic exchange occurs between Cu2 (face-cap) and Cu4 (vertex) mediated by a single μ-OPh bridge with a Cu–O–Cu angle of ~131°. The second strongest antiferromagnetic exchange interaction is between Cu3 (vertex) and Cu4 (vertex) mediated *via* a single μ-OH bridge with a Cu–O–Cu angle of ~126°. The two ferromagnetic exchange interactions occur between Cu1 (face cap) and Cu3 (vertex) mediated by μ-OH/μ-OPh bridges with an average Cu–O–Co angle of ~96° and a Cu–O–Cu–O dihedral angle of ~24°, and between Cu6 (vertex) and Cu8 (edge-cap) mediated by μ-O(NO_3)/OR groups with an average Cu–O–Co angle of ~98° and a Cu–O–Cu–O dihedral angle of ~17°. A detailed examination of the structure reveals that the sign and magnitude of J strongly depends on both the Cu–O–Cu angle and the Cu–O–Cu–O dihedral angle.[30] Large Cu–O–Cu angles lead to strong antiferromagnetic exchange whose magnitude decreases with decreasing angle (Fig. S9†). The switch to ferromagnetic occurs at a Cu–O–Cu angle of ~97–99°.[1–6] A large Cu–O–Cu–O dihedral angle in conjunction with a small Cu–O–Cu angle results in accidental orbital orthogonality (a counter complementarity effect arising from the presence of two different bridging ligands) which leads to a weak ferromagnetic interaction. DFT calculated spin density analysis (Fig. S10–S13†) suggests strong spin delocalisation with spin densities on the Cu^{II} ions of between 0.391–0.673. The bridging hydroxides/phenolic O-atoms have the largest spin density among the coordinating atoms, consistent with the strongest antiferromagnetic exchange through these moieties. The pattern of calculated exchange interactions (Table S2†) and the spin density analysis therefore strongly suggests the presence of spin frustration between the face-capping Cu ions housed in the calixarene polyphenolic pockets and the Cu ions at the vertices of the square prism. The small spin density of the N-atom of the nitrate points to a small, near-negligible, exchange through the Cu–O–N–O–Cu pathway (Fig. S14†).

Conclusions

The reaction between $Cu(NO_3)_2{\cdot}3H_2O$ and 2,2′-bis-*p*-^{t}Bu-calix[4]arene (H_8L) in a basic dmf/MeOH mixture and in the presence of the co-ligand Me-deaH_2 results in the formation of the complex $[Cu^{II}_{16}(L)_2(Me\text{-}dea)_4(NO_3)_2(OH)_4(dmf)_3(MeOH)(H_2O)_2](H_6L){\cdot}16dmf{\cdot}4H_2O$. Its metallic skeleton describes a tetra-capped square prism, [Cu_{12}], with two additional edge-capping [Cu_2] units introduced by the co-ligand sitting above and below the "upper" and "lower" square faces. The cage structure is held together internally *via* a combination of bridging hydroxides and nitrates, and externally by the two bis-*p*-^{t}Bu-calix[4]arenes. The structural similarity of [Cu_{16}] to [Cu_{13}], a centred, tetra-capped square prism also built with H_8L (in the absence of co-ligands), and [Cu_9], a tri-capped trigonal prism built with H_4TBC[4], reflects the dominant structure-directing role played by the calix[*n*]arene ligands. Magnetic susceptibility measurements reveal strong antiferromagnetic exchange interactions between neighbouring Cu^{II} ions within the central [Cu_{12}] tetra-capped square prism and between the Cu^{II} ions in the prism and the caps ($J = -122 \pm 12$ cm^{-1}), and strong ferromagnetic exchange between the Cu^{II} ions in the caps ($J' = +22 \pm 8$ cm^{-1}), leading to a ground state of $S = 1$. DFT calculations reveal a strong dependence of J on both the Cu–O–Cu and O–Cu–O–Cu angles, and suggest significant spin frustration in the central [Cu_{12}] tetra-capped square prism. Magnetisation and EPR data suggest the presence of significant ZFS in the $S = 1$ ground state, originating from anisotropic components of the exchange interaction. It will be interesting to examine the effect of extending the bridge length between the H_4TBC[4] moieties in bis-calix[4]arene ligands and/or of increasing the size of the calix[*n*]arene macrocycle, *e.g.* to *p*-^{t}Bu-calix[8]arene, on cage nuclearity and topology. Expansion into Cu-4f chemistry also promises the discovery of some interesting cages. This work is currently in progress.

Author contributions

LRBW, MC performed the synthetic chemistry and measured the magnetic data. LRBW and SP fitted the magnetic data. SJT/SJD collected and solved the XRD data. AB, MS and EJLM collected and analysed the EPR data. MKS performed theoretical calculations. SJD and EKB conceived the idea. All authors wrote/edited the manuscript.

Conflicts of interest

There are no conflicts to declare.

Acknowledgements

The authors thank the EPSRC for funding a studentship (LRBW) and grant EP/N01331X/1 (MC), and for funding of the EPSRC EPR National Research Facility (EP/W014521/1 and EP/V035231/1).

This research used resources of the Advanced Light Source, which is a DOE Office of Science User Facility under contract no. DE-AC02-05CH11231. For the purpose of open access, the author has applied a Creative Commons Attribution (CC BY) license to any Author Accepted Manuscript version arising from this submission.

Notes and references

1 B. Bleaney and K. D. Bowers, *Proc. R. Soc. London, Ser. A*, 1952, **A214**, 451.
2 W. H. Crawford, H. W. Richardson, J. R. Wasson, D. J. Hodgson and W. E. Hatfield, *Inorg. Chem.*, 1976, **15**, 2107.
3 W. E. Hatfield, *Comments Inorg. Chem.*, 1981, **1**, 105.
4 W. E. Marsh, K. C. Patel, W. E. Hatfield and D. J. Hodgson, *Inorg. Chem.*, 1983, **22**, 511.
5 C. P. Landee and R. E. Greeney, *Inorg. Chem.*, 1986, **25**, 3371.
6 S. S. Tandon, L. K. Thompson, M. E. Manuel and J. N. Bridson, *Inorg. Chem.*, 1994, **33**, 5555.
7 R. Boča, L. Dlhan, G. Mezei, T. Ortiz-Perez, R. G. Raptis and J. Telser, *Inorg. Chem.*, 2003, **42**, 5801.
8 J. Tercero, E. Ruiz, S. Alvarez, A. Rodriguez-Fortea and P. Alemany, *J. Mater. Chem.*, 2006, **16**, 2729.
9 E. Colacio, J. M. Dominguez-Vera, J.-P. Costes, R. Kivekas, J.-P. Laurent, J. Ruiz and M. Sundberg, *Inorg. Chem.*, 1992, **31**, 774.
10 O. Kahn, J. Galy, Y. Journaux, J. Jaud and I. Morgenstern-Badarau, *J. Am. Chem. Soc.*, 1982, **104**, 2165.
11 G. Rajaraman, F. Totti, A. Bencini, A. Caneschi, R. Sessoli and D. Gatteschi, *Dalton Trans.*, 2009, 3153.
12 A. Escuer, G. Vlahopoulou, F. Lloret and F. A. Mautner, *Eur. J. Inorg. Chem.*, 2014, 83.
13 M. Kohno, O. A. Starykh and L. Balents, *Nat. Phys.*, 2007, **3**, 790.
14 I. Bento, L. O. Martins, G. G. Lopes, M. A. Carrondo and P. F. Lindley, *Dalton Trans.*, 2005, 3507.
15 M. Murugesu, R. Clérac, C. E. Anson and A. K. Powell, *Inorg. Chem.*, 2004, **43**, 7269.
16 (*a*) S. M. Taylor, R. D. McIntosh, S. Piligkos, S. J. Dalgarno and E. K. Brechin, *Chem. Commun.*, 2012, **48**, 11190; (*b*) S. M. Taylor, R. D. McIntosh, C. M. Beavers, S. J. Teat, S. Piligkos, S. J. Dalgarno and E. K. Brechin, *Chem. Commun.*, 2011, **47**, 1440; (*c*) M. Coletta, S. Sanz, E. K. Brechin and S. J. Dalgarno, *Dalton Trans.*, 2020, **49**, 9882; (*d*) M. Coletta, S. Sanz, L. J. McCormick, S. J. Teat, E. K. Brechin and S. J. Dalgarno, *Dalton Trans.*, 2017, **46**, 16807; (*e*) G. Karotsis, S. J. Teat, W. Wernsdorfer, S. Piligkos, S. J. Dalgarno and E. K. Brechin, *Angew. Chem., Int. Ed.*, 2009, **48**, 8285; (*f*) S. M. Taylor, G. Karotsis, R. D. McIntosh, S. Kennedy, S. J. Teat, C. M. Beavers, W. Wernsdorfer, S. Piligkos, S. J. Dalgarno and E. K. Brechin, *Chem. – Eur. J.*, 2011, **17**, 7521; (*g*) M. A. Palacios, R. McLellan, C. M. Beavers, S. J. Teat, H. Weihe, S. Piligkos, S. J. Dalgarno and E. K. Brechin, *Chem. – Eur. J.*, 2015, **21**, 11212; (*h*) L. R. B. Wilson, M. Coletta, M. Evangelisiti, S. Piligkos, S. J. Dalgarno and E. K. Brechin, *Dalton Trans.*, 2022, **51**, 4213.
17 G. Karotsis, S. Kennedy, S. J. Dalgarno and E. K. Brechin, *Chem. Commun.*, 2010, **46**, 3884.
18 L. T. Carroll, P. Aru Hill, C. Q. Ngo, K. P. Klatt and J. L. Fantini, *Tetrahedron*, 2013, **69**, 5002.
19 R. McLellan, M. A. Palacios, C. M. Beavers, S. J. Teat, S. Piligkos, E. K. Brechin and S. J. Dalgarno, *Chem. – Eur. J.*, 2015, **21**, 2804.
20 (*a*) L. Noodleman and D. A. Case, *Adv. Inorg. Chem.*, 1992, **38**, 423; (*b*) L. Noodleman and E. R. Davidson, *Chem. Phys.*, 1986, **109**, 131; (*c*) L. Noodleman, *J. Chem. Phys.*, 1981, **74**, 5737; (*d*) L. Noodleman and J. G. Norman, *J. Chem. Phys.*, 1979, **70**, 4903.
21 M. J. Frisch, G. W. Trucks, H. B. Schlegel, G. E. Scuseria, M. A. Robb, J. R. Cheeseman, G. Scalmani, V. Barone, B. Mennucci, G. A. Petersson, H. Nakatsuji, M. Caricato, X. Li, H. P. Hratchian, A. F. Izmaylov, J. Bloino, G. Zheng, J. L. Sonnenberg, M. Hada, M. Ehara, K. Toyota, R. Fukuda, J. Hasegawa, M. Ishida, T. Nakajima, Y. Honda, O. Kitao, H. Nakai, T. Vreven, J. A. Montgomery, J. E. Peralta, F. Ogliaro, M. Bearpark, J. J. Heyd, E. Brothers, K. N. Kudin, V. N. Staroverov, R. Kobayashi, J. Normand, K. Raghavachari, A. Rendell, J. C. Burant, S. S. Iyengar, J. Tomasi, M. Cossi, N. Rega, J. M. Millam, M. Klene, J. E. Knox, J. B. Cross, V. Bakken, C. Adamo, J. Jaramillo, R. Gomperts, R. E. Stratmann, O. Yazyev, A. Austin, J. R. Cammi, C. Pomelli, J. W. Ochterski, R. L. Martin, K. Morokuma, V. G. Zakrzewski, G. A. Voth, P. Salvador, J. J. Dannenberg, S. Dapprich, A. D. Daniels, Ö. Farkas, J. B. Foresman, J. V. Ortiz, J. Cioslowski and D. J. Fox, *Gaussian 09, Revision E.01*, Wallingford CT, 2013.
22 (*a*) C. Lee, W. Yang and R. G. Parr, *Phys. Rev. B: Condens. Matter*, 1988, **37**, 785; (*b*) A. D. Becke, *J. Chem. Phys.*, 1993, **98**, 5648; (*c*) A. D. Becke, *J. Chem. Phys.*, 1993, **98**, 1372; (*d*) P. J. Stephens, F. J. Devlin, C. F. Chabalowski and M. J. Frisch, *J. Phys. Chem.*, 1994, **98**, 11623.
23 (*a*) A. Schäfer, H. Horn and R. Ahlrichs, *J. Chem. Phys.*, 1992, **97**, 2571; (*b*) A. Schäfer, C. Huber and R. Ahlrichs, *J. Chem. Phys.*, 1994, **100**, 5829; (*c*) G. E. Scuseria and H. F. Schaefer, III, *J. Chem. Phys.*, 1989, **90**, 3700.
24 (*a*) E. K. Brechin, D. J. Cutler, M. Coletta, M. Singh, A. B. Tsanai, L. J. McCormick McPherson, S. Coles and J. Schnack, *Dalton Trans.*, 2022, **51**, 8945; (*b*) M. Coletta, T. G. Tziotzi, M. Gray, G. S. Nichol, M. K. Singh, C. J. Milios and E. K. Brechin, *Chem. Commun.*, 2021, **57**, 4122; (*c*) D. J. Cutler, M. K. Singh, G. S. Nichol, M. Evangelisti, J. Schnack, L. Cronin and E. K. Brechin, *Chem. Commun.*, 2021, **57**, 8925; (*d*) S. S. Woodhouse, T. N. Dais, E. H. Payne, M. K. Singh, E. K. Brechin and P. G. Plieger, *Dalton Trans.*, 2021, **50**, 5318; (*e*) M. K. Singh and G. Rajaraman, *Inorg. Chem.*, 2019, **58**, 3175; (*f*) C. McDonald, S. Sanz, E. K. Brechin, M. K. Singh, G. Rajaraman, D. Gaynor and L. F. Jones, *RSC Adv.*, 2014, **4**, 38182; (*g*) S. Hazra, S. Bhattacharya, M. K. Singh,

L. Carrella, E. Rentschler, T. Weyhermueller, G. Rajaraman and S. Mohanta, *Inorg. Chem.*, 2013, **52**, 12881; (*h*) A. E. Dearle, D. J. Cutler, H. W. L. Fraser, S. Sanz, E. Lee, S. Dey, I. F. Diaz-Ortega, G. S. Nichol, H. Nojiri, M. Evangelisti, G. Rajaraman, J. Schnack, L. Cronin and E. K. Brechin, *Angew. Chem., Int. Ed.*, 2019, **58**, 16903; (*i*) K. R. Vignesh, S. K. Langley, K. S. Murray and G. Rajaraman, *Chem. – Eur. J.*, 2015, **21**, 2881; (*j*) P. A. Tsami, T. G. Tziotzi, A. B. Canaj, M. K. Singh, S. J. Dalgarno, E. K. Brechin and C. J. Milios, *Dalton Trans.*, 2022, **51**, 15128.

25 S. Shinkai, K. Araki, P. D. J. Grootenhuis and D. N. Reinhoudt, *J. Chem. Soc., Perkin Trans.*, 1991, **2**, 1883.

26 L. N. Dawe and L. K. Thompson, *Angew. Chem., Int. Ed.*, 2007, **46**, 7440; Y. Li, D. Li, J. Xu, H. Hao, S. Wang, J. Dou, T. Hu and X. Bu, *Dalton Trans.*, 2014, **43**, 15708; A. Adhikary, S. Goswami, J. A. Sheikh and S. Konar, *Eur. J. Inorg. Chem.*, 2014, 963; T. Liu, T. C. Stamatatos, K. A. Abboud and G. Christou, *Dalton Trans.*, 2010, **39**, 3554; V. Chandrasekhar and L. Nagarajan, *Dalton Trans.*, 2009, **34**, 6712; G. A. Craig, M. Schutze, D. Aguila, O. Roubeau, J. Ribas-Arino, S. Vela, S. J. Teat and G. Aromí, *Inorg. Chem.*, 2014, **53**(7), 3290; A. K. Kostopoulos, A. D. Katsenis, J. M. Frost, V. G. Kessler, E. K. Brechin and G. S. Papaefstathiou, *Chem. Commun.*, 2014, **50**, 15002; T. Zhao, X. Jing, J. Wang, D. Wang, G. Li, Q. Huo and Y. Liu, *Cryst. Growth Des.*, 2012, **12**, 5456; Y. Bai, V. Tangoulis, R. Huang, L. Zheng and J. Tao, *Chem. – Eur. J.*, 2009, **15**, 2377; X. Zhang, T. Han, Q. Zou, R. Zhu, J. Wang and Z. Li, *Z. Anorg. Allg. Chem.*, 2016, **642**, 4; P. Klüfers and J. Schumacher, *Angew. Chem., Int. Ed. Engl.*, 1995, **34**, 2119.

27 W. H. Press, S. A. Teukolsky, W. T. Vetterling and B. P. Flannery, *Numerical recipes in C: The Art of Scientific Computing*, Cambridge University Press, Cambridge, 2nd edn, 1992.

28 A. Bencini and D. Gatteschi, *Electron Paramagnetic Resonance of Exchange Coupled Systems*, Springer, Heidelberg, 1990.

29 (*a*) I. Dzyaloshinskii, *J. Phys. Chem. Solids*, 1958, **4**, 241; (*b*) T. Moriya, *Phys. Rev.*, 1960, **120**, 91; (*c*) S. Ferrer, F. Lloret, E. Pardo, J. M. Clemente-Juan, M. Liu-González and S. García-Granda, *Inorg. Chem.*, 2012, **51**, 985; (*d*) M.-A. Bouammalim, N. Suaud, N. Guihéry and R. Maurice, *Inorg. Chem.*, 2022, **61**, 12138; (*e*) J. Yoon and E. Solomon, *Coord. Chem. Rev.*, 2007, **251**, 379; (*f*) E. J. L. McInnes and D. Collison, *eMagRes*, 2016, **5**, 1445.

30 E. Ruiz, P. Alemany, S. Alvarez and J. Cano, *J. Am. Chem. Soc.*, 1997, **119**, 1297.